PHYSICAL REVIEW E **85**, 051309 (2012)

Relation between self-organized criticality and grain aspect ratio in granular piles

D. V. Denisov, Y. Y. Villanueva, K. A. Lőrincz, S. May, and R. J. Wijngaarden
Division of Physics, Faculty of Sciences, Vrije Universiteit, De Boelelaan 1081, 1081HV Amsterdam, The Netherlands
(Received 6 February 2012; published 22 May 2012)

We investigate experimentally whether self-organized criticality (SOC) occurs in granular piles composed of different grains, namely, rice, lentils, quinoa, and mung beans. These four grains were selected to have different aspect ratios, from oblong to oblate. As a function of aspect ratio, we determined the growth (β) and roughness (α) exponents, the avalanche fractal dimension (D), the avalanche size distribution exponent (τ), the critical angle (γ), and its fluctuation. At superficial inspection, three types of grains seem to have power-law-distributed avalanches with a well-defined τ. However, only rice is truly SOC if we take three criteria into account: a power-law-shaped avalanche size distribution, finite size scaling, and a universal scaling relation relating characteristic exponents. We study SOC as a spatiotemporal fractal; in particular, we study the spatial structure of criticality from local observation of the slope angle. From the *fluctuation* of the slope angle we conclude that greater fluctuation (and thus bigger avalanches) happen in piles consisting of grains with larger aspect ratio.

DOI: 10.1103/PhysRevE.85.051309 PACS number(s): 45.70.Ht, 05.65.+b

I. INTRODUCTION

For quite a long time scientists have studied the phenomenon of self-organized criticality (SOC) [1], which manifests itself in various processes: earthquakes [2], landslides [3], forest fires [4], rice piles [5], magnetic avalanches in superconductors [6], evolutionary bursts [7], and financial markets [8]. Recently it was shown [9] that sheared granular materials at high packing fractions can deform via slip avalanches. This system might also be modeled as SOC.

In a SOC system, energy is added to the system at a low rate, leading to the accumulation of instability. This instability is later released in abrupt events of all sizes, usually called avalanches. One of the characteristics of SOC is a power-law distribution of avalanche sizes, meaning that quite big and even system-wide avalanches have a not negligible probability of happening. Often such large events have a catastrophic nature (earthquakes, avalanches, forest fires, etc.), and, of course, it will be beneficial in general to find a way to prevent them. Many attempts have been undertaken to control avalanches, but the SOC behavior has proven to be very hard to suppress.

Avalanches in sand piles as the most commonly used paradigm for SOC behavior have been recently put under question. Sand pile experiments have not shown size distributions consistent with a power law, which is obligatory for the presence of SOC in the system [10]. In our experiments, to study avalanches in a controllable environment, instead of sand, we use different types of grains: rice, lentils, quinoa, and mung beans. These four grains were selected to have different aspect ratios, from oblong to oblate. It was found numerically in the anisotropic Oslo model [11] that anisotropy introduced to sandpile systems changes the critical exponents. Numerically the anisotropy can be introduced by changing the toppling rules in the system, but experimentally one cannot change the toppling rules directly. However, we can change the grain aspect ratio and check the changes in critical exponents.

Numerical and experimental studies have been performed on packing fraction and jamming of grains with different aspect ratios [12–15]. It was shown that grains with high and low aspect ratio can form structures with higher volume fractions compared to the structures formed from spherical grains. Moreover it was shown that long thin rods are able to jam into a solidlike state [13], which can strongly influence the avalanche behavior in such systems. Front velocity, area, and height of avalanches on a rough inclined plane have been already investigated experimentally for different grain shapes [16].

In this paper we are investigating the surface avalanches in granular piles and the dependence of their size distributions and critical exponents on the grain aspect ratio. To gather enough avalanche statistics, the experiments on each different type of grain lasted more than 500 h. It was found that the piles of rice clearly follow a power-law distribution of avalanche sizes and that quinoa piles definitely do not have such a power-law distribution. Avalanches in lentils and mung beans piles look at first glance like they obey the power-law behavior of avalanche size distribution, but further study shows that these systems are not SOC.

In Sec. II details of our grain pile experiments are given. In Sec. III we present results of our experiments and check the piles for SOC behavior using different methods: power-law distribution of avalanche size, universal exponent scaling relation (UESR) of characteristic exponents, and finite size scaling [17]. In Sec. IV we view SOC as a spatiotemporal fractal; in particular we study the spatial structure of criticality from local observation of the slope angle. We look into the fluctuations of the slope angle and its dependence on the aspect ratio of the grains. The relation between global and local critical angles is considered. Final conclusions are presented in Sec. V.

II. EXPERIMENTAL DETAILS

Our experiments were carried out on three-dimensional piles of various grains: rice, quinoa, lentils, and mung beans (see Fig. 1). These particular grains are chosen for their different aspect ratios a, which are shown in Table I, although they also differ in other aspects, e.g., size, mass, and surface properties.

The pile is contained in a box with three closed sidewalls and a floor area of 1×1 m^2. The fourth side is open, where grains can leave the box unimpeded; for a figure of

FIG. 1. (Color online) Images of grains used in the experiments: rice, lentils, quinoa, and mung beans. The black line in each subfigure is a 10 mm scale bar.

the setup see Ref. [18]. At the opposite side, grains are added continuously and uniformly across the top of the pile at such a rate that the system is always in a slow-driving regime [19]. The three-dimensional shape of the grain pile is determined by monocular stereoscopy, using a pattern of red-green-blue lines projected onto the pile [18,20]. A charge-coupled device color camera with a resolution of 2560×1920 pixels captures images of the pile approximately every 15 seconds. The time interval between two images is much shorter than the interval between avalanches. These images are analyzed to deduce the three-dimensional pile surface topography and the avalanche size s as described in Refs. [18,20]. By subtracting the shape of the pile before and after an avalanche, the full three-dimensional shape of the avalanche is determined. The size of an avalanche is defined as the volume of grain displaced between two consecutive time steps. The experiments presented here have only the "type-I" boundary condition [21]; i.e., during the entire experiment the foot of the grain pile rests on the horizontal plane of the box and never comes close to its open edge.

For potential systems that can be modeled as a SOC, the probability density for the avalanche size distribution is usually checked for consistency with a power-law behavior:

$$P(s) \sim s^{-\tau}, \tag{1}$$

where the parameter τ is the avalanche size distribution exponent, characteristic for the chosen system. For example in the classical BTW sand pile models τ is very close to 1 [1,22], for the forest fires τ is close to 1.3 [4], and for earthquakes $\tau \sim 2$ [23] (note that in this paper we use the probability density to characterize the size distribution of our avalanches while in the earthquake literature mostly the distribution function is used, which has exponent -1).

TABLE I. Properties of rice, quinoa, lentils, and mung bean grains. An anisotropy parameter k is introduced to characterize the deviation of the grains from the spherical form [see Eq. (7)].

	Length (mm)	Diameter (mm)	Aspect ratio (a)	Anisotropy parameter (k)
Rice	7	2	3.50	3.50
Quinoa	1.13	1.56	0.73	1.37
Lentils	2.4	5	0.48	2.08
Mung beans	6	4	1.50	1.50

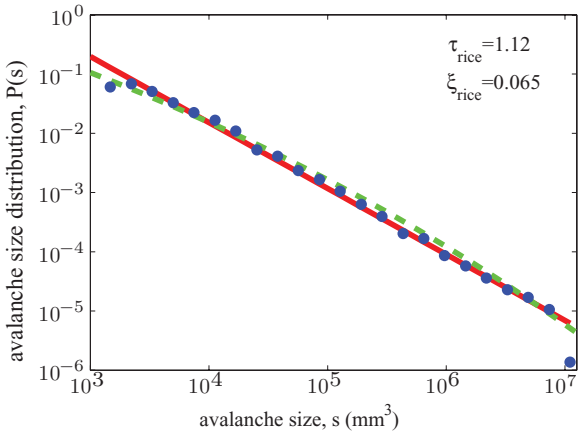

FIG. 2. (Color online) Avalanche size distribution for rice grains, which is consistent with a power law, $P(s) \sim s^{-\tau_{\text{rice}}}$ with $\tau_{\text{rice}} = 1.12$. A stretched exponential fit is also shown for comparison, $P(s) \sim \exp(-[s/s_0]^{\xi_{\text{rice}}})$ with $\xi_{\text{rice}} = 0.065$. Blue dots are experimental points, the solid red line is the power-law fit, and the dashed green line is the stretched exponential fit.

III. EXPERIMENTAL RESULTS

A. Avalanche size distribution

In order to obtain good avalanche size distribution statistics we have performed experiments until at least 1000 avalanche events were gathered for each type of grain. This corresponds to about 500 hours of measurement each. The different grain types vary significantly in shape and size (see Fig. 1 and Table I) leading to different avalanche behavior. It is well known that granular matter of high aspect ratio particles can behave as a cohesive material [24] and create a scaffolding structure. In other words, a pile of rice can grow very steep slopes, thus accumulating much "potential energy" or local instability, which can be later released via the avalanches. Indeed the avalanche size distribution for the rice pile shows a clear power-law behavior with very large maximum avalanche sizes (comparable to the box size); see Fig. 2 (the parameter ξ will be explained in the next section). To calculate τ from Eq. (1) we fit the avalanche size distribution with a straight line on a double logarithmic plot (the fit is the red solid line in Fig. 2). The slope of this linear function is τ. Due to the finite size of our experimental system the last point (or two) in the avalanche size distribution is usually not very well defined, so we are not taking it into account for the fit. For rice we thus obtain $\tau_{\text{rice}} = 1.12$.

In contrast to rice, quinoa grains are small, compact particles with highly curved (round) sides. The aspect ratio for quinoa is close to 0.73; i.e., due to their nearly perfect oval form they are, within the four types of grain investigated here, closest to a sphere. According to simulations [25] and our experimental results shown later in this paper (see Fig. 14), rounder particles (with a shape closer to a sphere) have a tendency to form less steeper piles. In such piles instability accumulation is less, leading to a smaller avalanche probability; large avalanches in particular are suppressed.

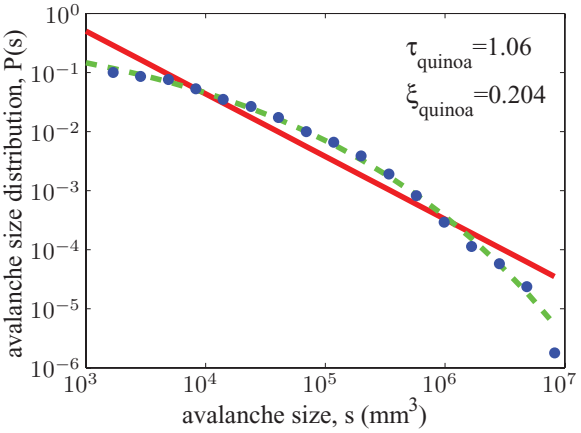

FIG. 3. (Color online) Avalanche size distribution for quinoa, which is a stretched exponential, $P(s) \sim \exp(-[s/s_0]^{\xi_{quinoa}})$ with $\xi_{quinoa} = 0.202$. A power-law fit is also shown for comparison, $P(s) \sim s^{-\tau_{quinoa}}$ with $\tau_{quinoa} = 1.06$. Blue dots are experimental points, the solid red line is the power-law fit, and the dashed green line is the stretched exponential fit.

Figure 3 shows the quinoa avalanche size distribution, which is definitely not a power law. We can still fit it with a power law (using all points except the very last one), obtaining $\tau_{quinoa} = 1.06$, but this value should not be taken seriously. Usually one is interested in the probability of the largest, devastating, events, for which case only the tail of the avalanche size distribution is fitted with a power law giving $\tau^{tail}_{quinoa} = 1.63$ (using the last seven points except the very last one). Note that $\tau^{tail}_{quinoa} = 1.63$ is much larger than τ_{rice}, indicating that the probability of large avalanches occurring in a quinoa pile is much smaller in comparison to the rice pile.

Lentils have an aspect ratio $a = 0.48$, and in contrast to the slightly oval form of the quinoa grains, the lentils are rather flat discs. A power law fits the avalanche size distribution quite well, giving $\tau_{lentils} = 1.15$; see Fig. 4.

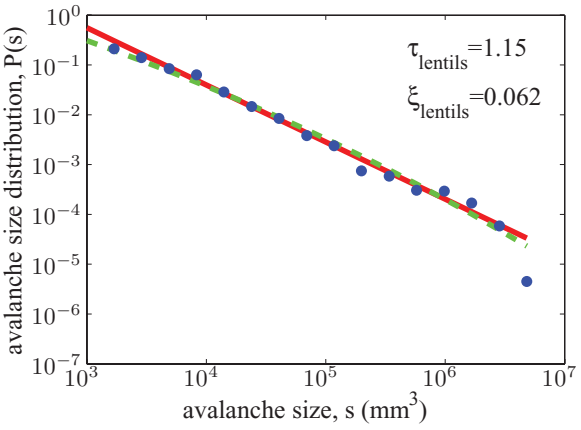

FIG. 4. (Color online) Avalanche size distribution for lentils, which is consistent with a power law, $P(s) \sim s^{-\tau_{lentils}}$ with $\tau_{lentils} = 1.15$. A stretched exponential fit is also shown for comparison, $P(s) \sim \exp(-[s/s_0]^{\xi_{lentils}})$ with $\xi_{lentils} = 0.062$. Blue dots are experimental points, the solid red line is the power-law fit, and the dashed green line is the stretched exponential fit.

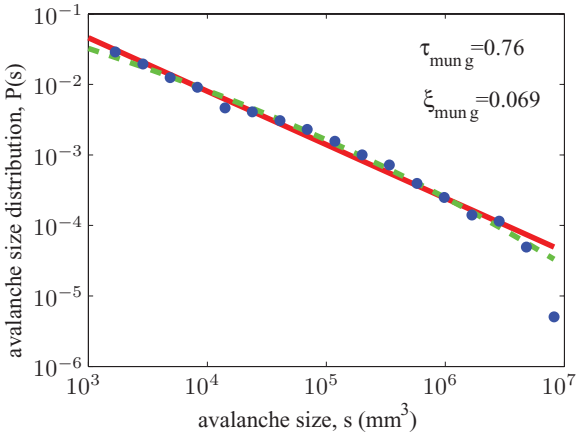

FIG. 5. (Color online) Avalanche size distribution for mung beans, which is consistent with a power law, $P(s) \sim s^{-\tau_{mung}}$ with $\tau_{mung} = 0.76$. A stretched exponential fit is also shown for comparison, $P(s) \sim \exp(-[s/s_0]^{\xi_{mung}})$ with $\xi_{mung} = 0.069$. Blue dots are experimental points, the solid red line is the power-law fit, and the dashed green line is the stretched exponential fit.

Mung beans have an aspect ratio $a = 1.50$, and the avalanche size distribution can be fitted quite well with a power law, although for small sizes, the fit is worse than for rice; see Fig. 5. We find $\tau_{mung} = 0.76$, the smallest value of all grains investigated here. Note that a smaller τ implies a larger relative probability of extreme events. This τ value less than unity is surprising in view of the different sandpile models [26–29] where τ is in the range 1–1.6. Also in general the τ cannot be less than unity for the whole range of s from zero to infinity, because for $\tau < 1$ the $P(s)$ is non-normalizable; see Ref. [30] for a discussion and possible solution. To compare τ_{mung} with that of the other grains, we nevertheless use an experimentally obtained value of $\tau_{mung} = 0.76$ in the measured range of s.

One could argue that the higher local stability due to the "scaffolding" structure of a rice pile leads to a greater accumulation of the potential energy and hence to a larger probability for extremely large avalanches. In view of our finding here, $\tau_{rice} > \tau_{mung}$, this assumption is not proven to be true. Later in this paper we will return to this question when we investigate the local slope distribution.

B. Stretched exponential analysis

It was shown by Feder [31] for quite a number of natural processes, which supposedly had SOC, that their event sizes are not power law distributed. Feder demonstrated that for these processes the event size distribution is fitted better by a stretched exponential, and hence they cannot be SOC.

To investigate whether a real power-law behavior is observed in the avalanche size distribution of the grains under consideration here, we perform, like Feder, also a stretched exponential fit (Figs. 2–5), using the formula

$$P(s) = A \exp(-[s/s_0]^{\xi}), \tag{2}$$

where ξ is the stretching exponent. Stretched exponential fits using Eq. (2) are shown in Figs. 2–5 by the dashed green lines. Table II shows the values of τ obtained from fitting Eq. (1) and ξ from Eq. (2).

TABLE II. Values of τ and ξ obtained by fitting Eqs. (1) and (2) to the avalanche size distribution of rice, quinoa, lentils, and mung beans. $\overline{R}^2$ shows the goodness of the corresponding fit.

	τ	$\overline{R}^2$ Power law	ξ	$\overline{R}^2$ Stretched exponential
Rice	1.12	0.998	0.065	0.997
Quinoa	1.06	0.947	0.202	0.997
Lentils	1.15	0.990	0.062	0.985
Mung beans	0.76	0.990	0.069	0.994

To decide which model fits our experimental size distribution best, we use the adjusted coefficient of determination $\overline{R}^2$as a goodness-of-fit parameter. Values of $\overline{R}^2$ are presented in Table II and show that judging by $\overline{R}^2$ only, a power law fits the rice and lentils data better, while a stretched exponential fits the quinoa and mung bean data better. Especially in the quinoa case the difference in $\overline{R}^2$ is very much in favor of the stretched exponential. However, the fact that $\xi \simeq 0.065$ and hence is very small for all cases except quinoa, means that the corresponding size distributions differ only very slightly from a power law. We note that if one would fit exact power-law data with Eq. (2), one would find values of ξ close to zero. We call ξ "small" if the stretched exponential fit is nearly a power law [32]. As a preliminary conclusion at this point we can say that the avalanche size distribution of rice and lentil piles shows a clear consistency with a power-law behavior. These are the grains with the largest ($a = 3.50$) and the smallest ($a = 0.48$) aspect ratio a. Quinoa certainly does not have a power-law distribution, while from all four grains it is closest to a sphere ($a = 0.73$). For mung beans (with $a = 1.50$) the power-law case is still undecided, and we need additional input. This is the subject of the next section.

C. Universal scaling relations

According to [17] it is not enough for a system to have a power-law distribution of event size to be SOC: If the system is truly SOC, then various universal exponent scaling relations should hold. Some of these relations are better accessible for experimental verification than others. Here we focus on the relation [17,33]

$$\alpha/\beta = D(2-\tau), \tag{3}$$

which we will refer to as UESR. Interestingly, this UESR relates surface exponents (l.h.s.) to avalanche exponents (r.h.s.); namely, the avalanche size distribution is characterized by τ [Eq. (1)], and the shape of individual avalanches is characterized by their fractal dimension D, while the surface of the pile is characterized by the roughness and growth exponents, namely, α and β.

To find α and β in our systems, we analyze the surface of our piles. Since we can precisely reconstruct the pile surface at 15-sec intervals during the experiment, we know the height of the pile $h(x,y,t)$ at every point of the pile as a function of time. We use the two-point correlation function of Barabasi to analyze the surface [33]:

$$C^2(\ell,t) = \langle[\delta h(x,y,t+t') - \delta h(x',y',t')]^2\rangle, \tag{4}$$

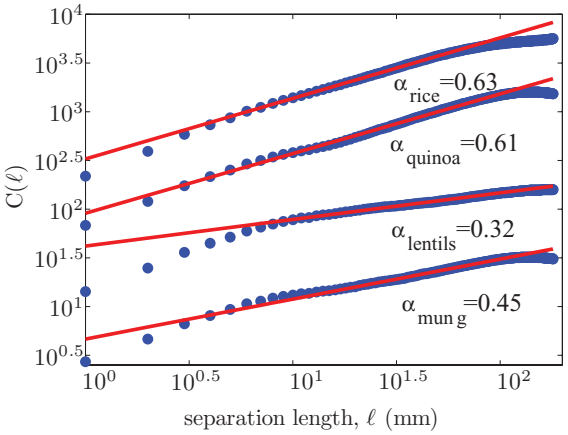

FIG. 6. (Color online) Determination of the roughness exponent from the two-point correlation function $C(\ell) \sim \ell^{\alpha}$, yielding $\alpha_{\text{rice}} = 0.63(4)$, $\alpha_{\text{quinoa}} = 0.61(4)$, $\alpha_{\text{lentils}} = 0.32(5)$, $\alpha_{\text{mung}} = 0.45(4)$. From top to bottom results are shown for rice, quinoa, lentils, and mung beans (curves have been shifted vertically for clarity). Blue dots are experimental points, the solid red line is the power-law fit.

where $\delta h(x,y,t') = h(x,y,t') - \overline{h}(t')$ and $\overline{h}(t')$ is the mean height of the surface at time t'. The correlation function scales as

$$C(\ell,0) = C(\ell) \sim \ell^{\alpha}, \tag{5}$$

$$C(0,t) = C(t) \sim t^{\beta}, \tag{6}$$

where $\ell = \sqrt{(x-x')^2 + (y-y')^2}$. To obtain $C(\ell,0)$ in Eq. (5) and calculate α we average Eq. (4) over all x',y' at a radius ℓ from (x,y) and then subsequently average over all time steps. To obtain $C(0,t)$ in Eq. (6) and evaluate β we average Eq. (4) over all points in the pile (x',y'), but time averaging is done over ensembles separated by a fixed time interval t.

The roughness exponent α was determined for every experimental run separately using Eq. (5) and then averaged over all experiments (more than 10) for each grain type. The average values of α with statistical error in brackets are shown in Table III. The corresponding power-law fits of Eq. (5) are presented in Fig. 6. Blue dots correspond to the experimental points, while the red line is the power-law fit.

For the determination of α we used the straight middle section. The deviation from power-law behavior at small $\ell \leqslant 3$ mm is due to the fact that subgrain length scales are reached. Large ℓ are not used for the fitting because finite system size effects are limiting the fluctuations. Note that an intrinsic width effect [33] would give an upward curvature effect contrary to the observed downward curvature.

Interestingly, the pile surface is smoothest for lentils ($\alpha_{\text{lentils}} = 0.32$), probably due to the specific "scale-like" arrangement of the disk-shaped particles. This may be related to the very dense packing observed for M&M candies [12].

On the other hand, rice has the irregular complex scaffolding surface structure of the elongated grains, and consequently rice has the largest roughness exponent $\alpha_{\text{rice}} = 0.63$. Naturally, mung beans with an intermediate shape, closer to a sphere, have the intermediate $\alpha_{\text{mung}} = 0.45$. Surprisingly, quinoa grains, which are even closer to spherical, have a quite large $\alpha_{\text{quinoa}} = 0.61$, comparable to the value for rice. Possibly this is

TABLE III. Universal exponents of rice, quinoa, lentils, and mung bean grains. Values in brackets show the error margin for τ, α, β and D^{exp}. The anisotropy parameter k is defined by Eq. (7).

	Aspect ratio (a)	Anisotropy parameter (k)	Avalanche size exponent (τ)	Roughness exponent (α)	Growth exponent (β)	Avalanche fractal dimensions (D^{exp})
Rice	3.50	3.50	1.12(1)	0.63(4)	0.34(2)	2.16(13)
Quinoa	0.73	1.37	1.06(6)	0.61(4)	0.42(4)	2.24(09)
Lentils	0.48	2.08	1.15(3)	0.32(5)	0.34(1)	2.11(10)
Mung beans	1.50	1.50	0.76(2)	0.45(4)	0.42(4)	2.18(11)

due to the fact that quinoa are the smallest and lightest grains, leading to a larger role of friction, which, like the scaffolding structure of rice, may have a stabilizing influence. The relation between roughness exponent α and aspect ratio a is shown in Fig. 7, where it is seen that lentils, mung beans, and rice follow a similar law, while quinoa is an exception.

The growth exponent β was calculated in a similar way as the roughness exponent α, now using Eq. (6). The growth exponent was determined using the whole duration of a single experiment and then averaged over all experiments for each grain type. The average value of β is shown in Table III. Figure 8 shows the corresponding power-law fits. Interestingly, for all grain types the power-law behavior is very well defined for $C(t)$ down to the smallest periods of time. At long time scales the correlation function starts to diverge from power-law behavior. Therefore the data of large correlation times were omitted from the fitting procedure.

The values of the growth exponent for rice and lentils are equal at $\beta = 0.34$, and the values for quinoa and mung beans are equal at $\beta = 0.42$. This similarity may be compared to the anisotropy parameter

$$k = \max(a, 1/a), \tag{7}$$

where a is the aspect ratio of the grains. For example $k_{\text{quinoa}} = 1.37$ is close to $k_{\text{mung}} = 1.5$, while rice and lentils are much more anisotropic with $k_{\text{rice}} = 3.5$ and $k_{\text{lentils}} = 2.08$ relatively.

The fractal dimension D^{exp} of the avalanches is calculated as follows. First, the three-dimensional shape of every avalanche that does not touch any wall of the system is determined from a subtraction of the pile surface before and after the avalanche. Then the fractal dimension of the avalanche is determined using the box counting method [34]. In this method, the number of boxes $N(L)$ which contain a part of the avalanche is a power-law function of the linear size of the box L:

$$N(L) \sim L^{-D^{\text{exp}}}.$$

For each individual avalanche, the box size ranged from 2 to 600 mm. The resulting fits are presented in Fig. 9.

To determine D^{exp} we used small values of L, since there are many boxes of small sizes, making an accurate covering of the avalanche by such boxes possible. However, large values L were not used for the fitting, because there are just a few number of boxes of such sizes, implying that the resolution in number of boxes becomes poor and an accurate covering is no longer achieved. In Table III, the values D^{exp} are an average over all fits for individual avalanches for a single grain type (with the error margin in brackets). Clearly the fractal dimension D^{exp} for all grain types is similar, with D^{exp} in the range 2.11–2.24.

Finally, after obtaining τ, α, β and D^{exp} from experiment, we can check the validity of the UESR [Eq. (3)]. For this

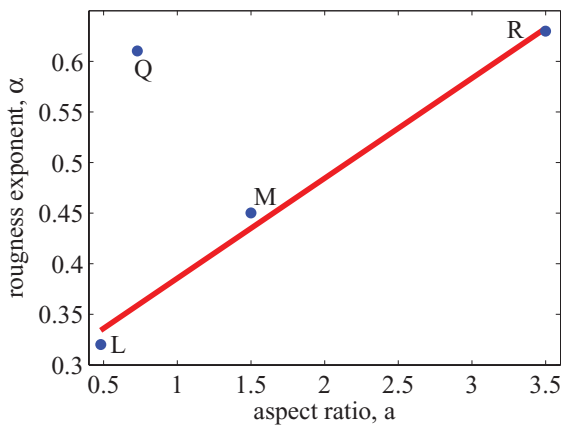

FIG. 7. (Color online) Dependence of roughness exponent α on the aspect ratio a for various grains. Blue dots are experimental points, while the solid red line indicates the approximate linear relation $\alpha(a)$ for lentils, mung beans, and rice. Labels R, Q, L, and M stand for rice, quinoa, lentils, and mung beans, respectively.

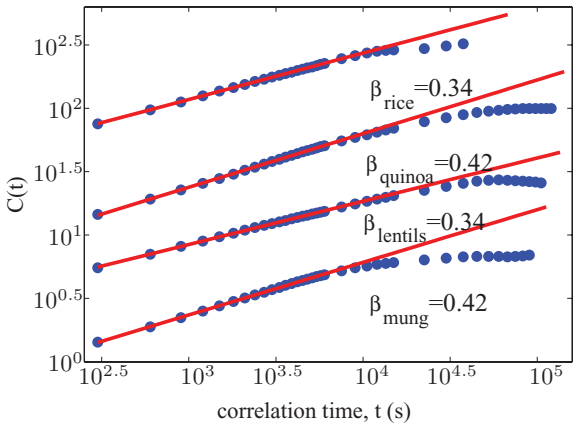

FIG. 8. (Color online) Determination of the growth exponent for all grains using the two-point correlation function $C(t) \sim t^{\beta}$, yielding $\beta_{\text{rice}} = 0.34(2)$, $\beta_{\text{quinoa}} = 0.42(4)$, $\beta_{\text{lentils}} = 0.34(1)$, $\beta_{\text{mung}} = 0.42(4)$. From top to bottom data is shown for rice, quinoa, lentils, and mung beans (data is shifted vertically for clarity). Blue dots are experimental points; the solid red line is a power-law fit.

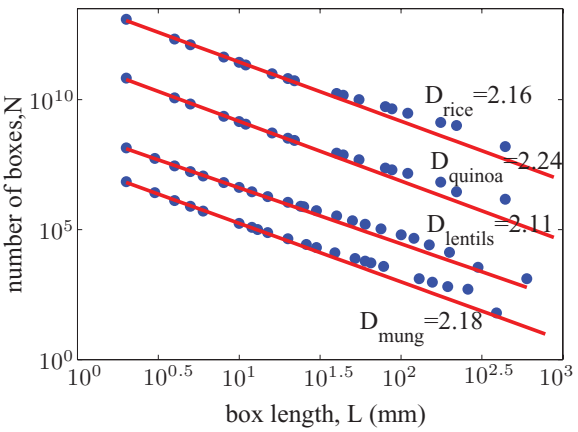

FIG. 9. (Color online) Determination of the avalanche fractal dimensions D^{exp} by the box counting method, by fitting to $N(L) \sim L^{-D^{\text{exp}}}$. We find $D^{\text{exp}}_{\text{rice}} = 2.16(13)$, $D^{\text{exp}}_{\text{quinoa}} = 2.24(09)$, $D^{\text{exp}}_{\text{lentils}} = 2.11(10)$, and $D^{\text{exp}}_{\text{mung}} = 2.18(11)$. From top to bottom results for rice, quinoa, lentils, and mung beans are shown (data are shifted vertically for clarity). Blue dots are experimental points; the solid red line is a power-law fit.

purpose, we use Eq. (3) to calculate D^{UESR} from τ, α, and β and subsequently compare D^{UESR} with D^{exp}. We find $D^{\text{UESR}}_{\text{rice}} = 2.08$, $D^{\text{UESR}}_{\text{quinoa}} = 1.53$, $D^{\text{UESR}}_{\text{lentils}} = 1.17$, $D^{\text{UESR}}_{\text{mung}} = 0.88$. The value $D^{\text{UESR}}_{\text{rice}} = 2.08$ corresponds nicely to $D^{\text{exp}}_{\text{rice}} = 2.16$; both are slightly larger than 2, which is a physically meaningful value. The unphysical $D^{\text{UESR}}_{\text{mung}} < 1$ and also $D^{\text{UESR}}_{\text{mung}} \neq D^{\text{exp}}_{\text{mung}}$, hence the violation of UESR, both imply separately that avalanches in mung bean piles are not SOC. For lentils we find the physically allowed value $D^{\text{UESR}}_{\text{lentils}} = 1.17$; however, this deviates so much from $D^{\text{exp}}_{\text{lentils}} = 2.11$ that we find again a violation of UESR, and hence lentil piles are not SOC. For quinoa, the values $D^{\text{UESR}}_{\text{quinoa}} = 1.53$ and $D^{\text{exp}}_{\text{quinoa}} = 2.24$ are quite different leading to the provisional conclusion that quinoa is not SOC. This becomes a firm conclusion after realizing that the avalanche size distribution of quinoa clearly is not a power law. Hence quinoa is also not SOC. At this point, after applying the universal exponent scaling relation analysis, we conclude that only rice piles can be truly modeled as SOC systems in the regime we observe.

D. Finite size scaling

Avalanches in SOC systems are fractal objects and hence a finite size scaling (FSS) analysis can be applied to them. So another way to check whether our piles display SOC behavior is to check whether FSS is obeyed. FSS requires that the avalanche size distribution $P(s,L)$ depends in a specific manner on the size of the total system:

$$P(s,L) = s^{-\tau} f(s/L^{D^{\text{exp}}}), \tag{8}$$

where $f(x)$ is an unknown function, constant up to some value (corresponding to the cutoff scale) and going smoothly, but fast to zero for large x. Usually for FSS analysis, experiments with different system sizes L are performed. However, this is difficult to implement in our case. Instead, we use a moving window of certain linear size L to scan the surface for avalanches. If an avalanche is detected and it fits within the window, then we take it into account for $P(s,L)$; otherwise it is ignored. By varying the window size L we obtain the avalanche size distribution for different system sizes $P(s,L)$ [20]. This $P(s,L)$ is checked for FSS behavior by plotting $s^{\tau} P(s,L)$ versus $s/L^{D^{\text{exp}}}$, i.e., by constructing the function $f(x)$ from experiment, using the experimental values for the parameters τ and D^{exp} as found from the analysis above. If our avalanches indeed obey FSS, then we should get a single curve $f(x)$.

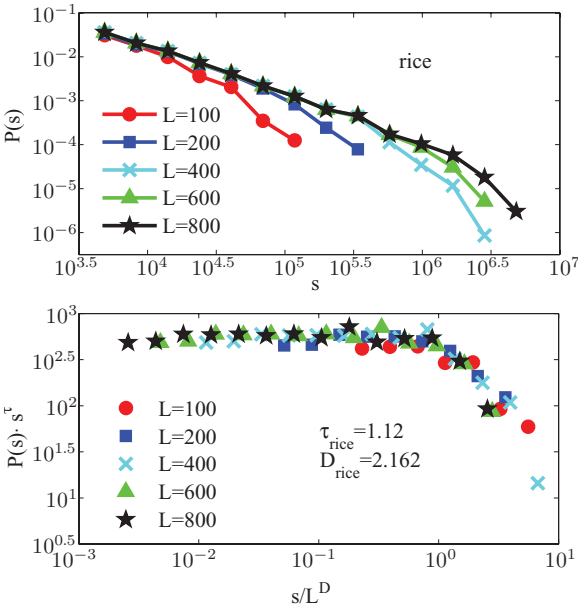

FIG. 10. (Color online) Top: Rice avalanche size distribution $P(s,L)$ for different system sizes $L = 100,200,400,600,800$ mm. Bottom: Corresponding finite size scaling data collapse.

Our FSS results are shown in Figs. 10–13. We used the values of τ and D^{exp} from Table III to build the function $f(x)$, shown in bottom parts of Figs. 10–13.

The nice data collapse for rice shows a clear constant $f(x)$ for small values of $x = s/L^{D^{\text{exp}}_{\text{rice}}}$ and well-defined tail, as expected (Fig. 10). Hence, it can be safely concluded that rice piles indeed can be modeled as SOC.

There is clearly no data collapse for quinoa (Fig. 11), as was expected, since the quinoa avalanche size distribution is not a power law but rather a stretched exponent. It should be mentioned, however, that a collapse to a single $f(x)$ for quinoa can be obtained with $\tau_{\text{quinoa}} = 0.7$ and $D_{\text{quinoa}} = 1.5$. Of course, these fitting parameters are very far from the experimentally obtained values, signifying again that quinoa piles are not SOC.

For lentils (Fig. 12) a good data collapse is obtained for the horizontal part, but not for the tail of the distribution where the data are scattered. This confirms that the lentil avalanche size distribution is indeed consistent with a power law, but that FSS cannot be applied to this system using the experimentally obtained $D^{\text{exp}}_{\text{lentils}}$, marking it as a weak or non-FSS.

For mung beans, the data collapse (Fig. 13) shows a small "hunch" in the horizontal part of the distribution. Only if we change the τ_{mung} value from the previously quoted value 0.76 to 0.65 do we get rid of this "hunch" and produce a very clear (horizontal part and tail) cutoff function $f(x)$. This is related to the previously mentioned deviation at small s in Fig. 5.

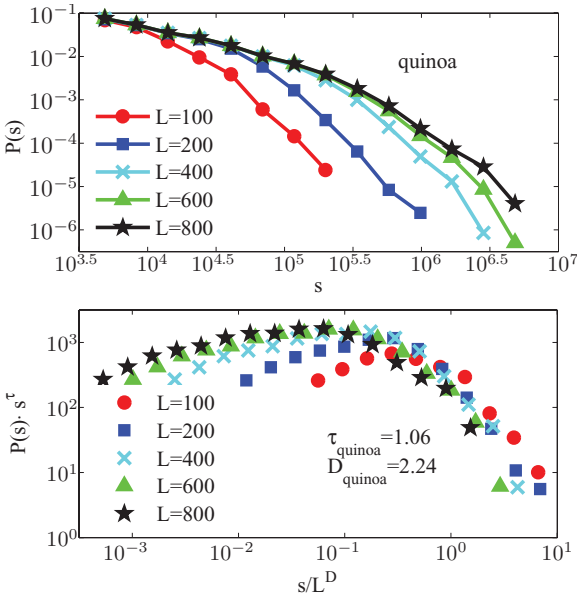

FIG. 11. (Color online) Top: Quinoa avalanche size distribution $P(s,L)$ for different system sizes $L = 100,200,400,600,800$ mm. Bottom: Corresponding finite size scaling data collapse.

The lowering of τ_{mung} to 0.65 makes the UESR [Eq. (3)] even worse. Hence, despite the power-law behavior of the avalanche size distribution and possibly FSS, we conclude that mung bean piles cannot be considered to be SOC systems.

Additionally for all grains we tried moment ratios FSS scaling [35], where only the τ parameter needs to be fitted. Essentially it provides the same results. In general, after applying FSS analysis, only rice is found to be SOC, confirming previous conclusions [21]. Quite obviously, FSS cannot be applied to quinoa avalanche size distributions, since

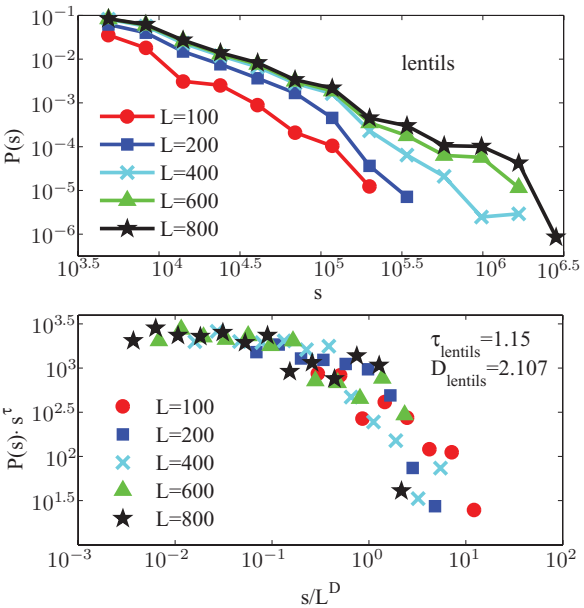

FIG. 12. (Color online) Top: Lentil avalanche size distribution $P(s,L)$ for different system sizes $L = 100,200,400,600,800$ mm. Bottom: Corresponding finite size scaling data collapse.

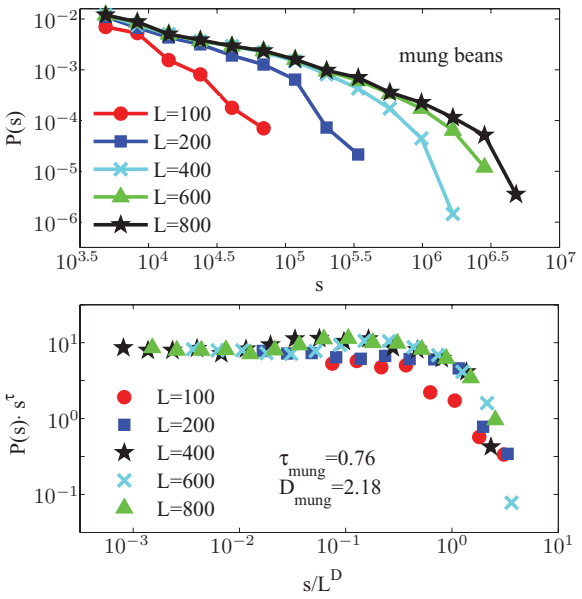

FIG. 13. (Color online) Top: Mung bean avalanche size distribution $P(s,L)$ for different system sizes $L = 100,200,400,600,800$ mm. Bottom: Corresponding finite size scaling data collapse.

they are not power laws. Lentils and mung beans turn out to be weak FSS, which together with our previous conclusions above signifies that they are not true SOC systems. Finally, we note that FSS is a stringent test for the fractal nature of the avalanches, even more than it is a test for SOC.

IV. CRITICAL ANGLES

A SOC system is a spatiotemporal fractal, with the punctuated behavior of the avalanches defining the temporal fractal character and their physical shape defining their spatial character. Although the system as a whole is always critical, avalanches may temporarily relax the system locally. By this mechanism, a SOC pile will have a spatially modulated critical structure, experimentally accessible by the observation of the slope angle.

The correlation between the angle of repose of the pile and the shape of the grains was investigated in Ref. [25] by simulation and in Ref. [16] by experiment. It was found that spherical grains have a lower angle of repose than nonspherical grains and that for nonspherical grains the angle of repose fluctuates much stronger. To check this finding in our experimental system we calculate the slope angle from the reconstructed images of our experiments; the results are shown in Fig. 14. The slope angle γ_{pile} for the whole pile was calculated as an average of the slope angles γ of small sections (approximately 3.5 cm $\times$ 3.5 cm), together covering the whole pile surface.

From Fig. 14 we find that the maximal slope angle is proportional to the anisotropy parameter k; see the left-hand panel of Fig. 15 and Table IV. Quinoa with k_{quinoa} closest to 1 has the smallest critical angle, while rice with $k_{\text{rice}} = 3.5$ has highest critical angle. This finding seems in agreement with the conjecture above that a large anisotropy parameter of the grains enables larger local slopes and a larger accumulation of instability. By defining the time T as the

TABLE IV. Granular pile angle properties for rice, quinoa, lentils, and mung beans. $\gamma_{\text{pile}}^{\max}$ is the highest angle that is reached in the experimental 1×1 m^2 pile before a system-wide avalanche occurs. $\gamma_{\text{local}}^{\max}$ is the highest angle measured locally. Angle fluctuations $\Delta\gamma_{\text{pile}}$ are defined as deviation from mean slope angle for the duration of the experiment. The anisotropy parameter k is defined by Eq. (7).

	Aspect ratio (a)	Anisotropy parameter (k)	Critical angle (pile) ($\gamma_{\text{pile}}^{\max}$) (°)	Angle fluctuations ($\Delta\gamma_{\text{pile}}$) (°)	Critical angle (local) ($\gamma_{\text{local}}^{\max}$) (°)
Rice	3.50	3.50	37	1.00	47
Quinoa	0.73	1.37	28.5	0.61	37
Lentils	0.48	2.08	30	0.50	40.5
Mung beans	1.50	1.50	29	0.82	35

whole duration of an experiment, we can introduce the slope angle *fluctuations* $\Delta\gamma_{\text{pile}} := [\frac{1}{T}\sum_{t=1}^{T}(\gamma_{\text{pile}}(t) - \langle\gamma_{\text{pile}}\rangle_t)^2]^{1/2}$, which are not influenced by the anisotropy parameter k, but by the aspect ratio a itself (see right-hand panel of Fig. 15 and Table IV). For grains with $a > 1$ (the elongated grains of rice and mung beans), we find quite large fluctuations, corresponding to big, system-wide avalanches. By contrast, for quinoa with a_{quinoa} close to 1, we observe small angle fluctuations, in agreement with the result of Ref. [25]. In contrast to this simulation [25], we do observe rare large jumps in angle. This difference may be due to the fact that in the simulation, only a rather small number of particles (up to 1800) was used. Even more interestingly, lentils show the smallest fluctuations of the angle. Even the rare big jumps that are observed in quinoa are absent for lentils. This may be due to their disk shape, which enables the creation of a pile with a very compact packing in the vertical direction (see, e.g., Ref. [12]). Thus even when an avalanche occurs, the height profile does not change much.

We conclude that the angle $\gamma_{\text{pile}}^{\max}$ is proportional to the anisotropy parameter k. In other words, it depends on the deviation of the grains from the spherical shape; see Fig. 15 (left). On the other hand, the angle fluctuations $\Delta\gamma_{\text{pile}}$ depend directly on aspect ratio a, although in a strongly nonlinear manner $\Delta\gamma_{\text{pile}} \sim \log a$; see Fig. 15 (right).

In view of the spatiotemporal character of avalanches discussed above, it is interesting to monitor not only the average slope of the pile $\gamma_{\text{pile}}^{\max}$, but also the local slopes γ_{local},

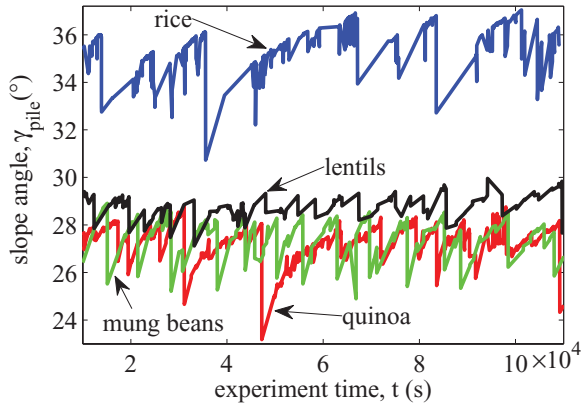

FIG. 14. (Color online) Average slope angle γ_{pile} as a function of time t (seconds) for different types of grains. Data for rice are shown in blue, for quinoa in red, for lentils in black, and for mung beans in green.

which can be significantly larger. Usually, at positions in the pile where the slope has the largest angle, a new avalanche will start. Figure 16(b) shows an example of such avalanche in rice, which changed the pile from the state (a) to the state (c). Blue areas in Fig. 16(b) correspond to removed grains, red areas correspond to added grains, while green areas correspond to zero net change. Green areas are usually between red and blue areas or in areas completely untouched by the avalanche, for example, in the lower-left corner in Fig. 16(b). Figures 16(a) and (c) show angles measured locally (i.e. determined from approximately 3.5 cm × 3.5 cm sections) in a rice pile before and after a given avalanche (the value of the angle is coded by color).

The global value of $\gamma_{\text{pile}}^{\max}(rice)$ shown in Fig. 14 is close to 37°. However, it is seen from Figs. 16(a) and 16(c) that locally angles can reach much higher values. In Fig. 16 the lower angle threshold for the color scale was set to 37° to visualize only angles higher than $\gamma_{\text{pile}}^{\max}(rice)$. In quite large areas of the pile surface local angles exceed $\gamma_{\text{pile}}^{\max}(rice)$. It was observed that when the local angle reaches approximately $\gamma_{\text{local}}^{\max} = 44 - 47°$, the avalanche starts from the corresponding local area. We define the value of local angle always leading to an avalanche as the local critical angle. In the case of rice this is 47°. However, depending on local conditions,

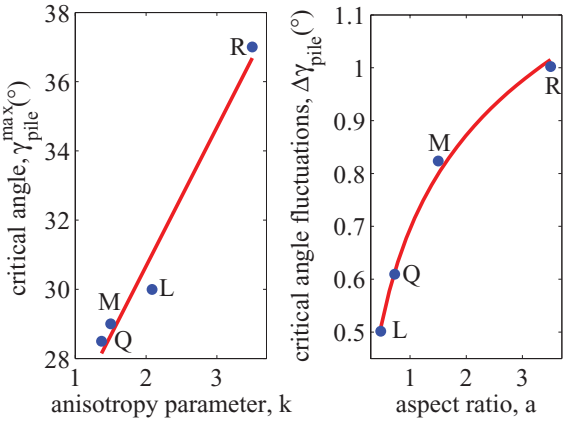

FIG. 15. (Color online) Left: Dependence of the critical angle $\gamma_{\text{pile}}^{\max}$ on the anisotropy parameter k [defined by Eq. (7)] for the various grains. Right: Dependence of the angle fluctuations $\Delta\gamma_{\text{pile}}$ on the aspect ratio a for the various grains. Blue dots are experimental points, while solid red lines are a linear (left) and logarithmic (right) fits, showing the approximate proportionalities $\gamma_{\text{pile}}^{\max} \sim k$ and $\Delta\gamma_{\text{pile}} \sim \log a$. Labels R, Q, L, and M stand for rice, quinoa, lentils, and mung beans, respectively.

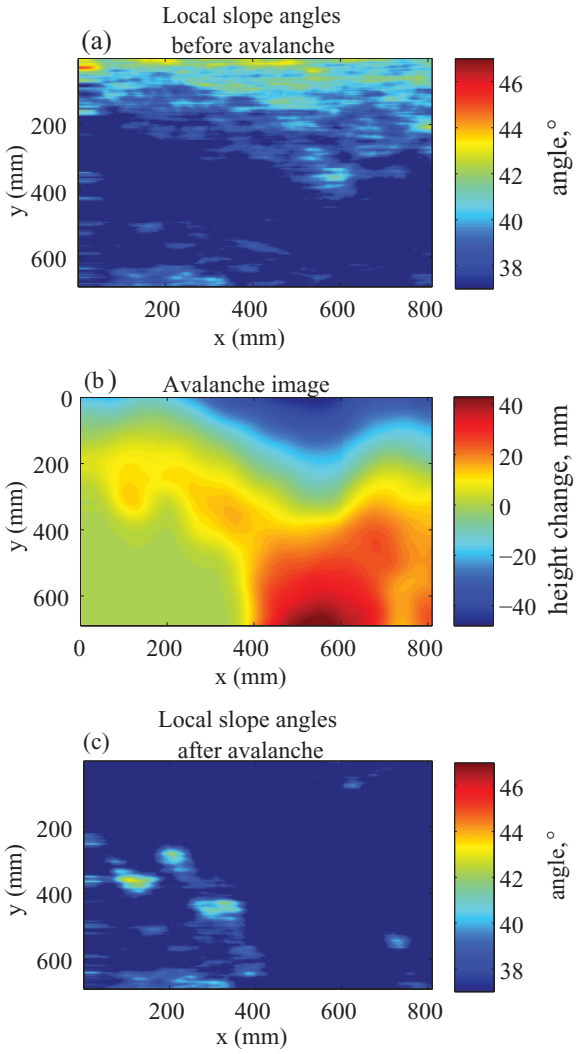

FIG. 16. (Color online) Distribution of the local angles γ on the rice pile surface, (a) before a particular avalanche, (c) after this avalanche. Deep blue (dark) indicates relaxed part of the pile, and other colors (bright) indicate part of the pile where $\gamma > \gamma_{\text{pile}}^{\max}$. (b) Change of the pile height by this avalanche is shown. The avalanche moves downward in the figure (from small to large y). Blue (upper dark gray part of the image) indicates regions where particles are removed, and red (lower part of the image) indicates regions where particles are added.

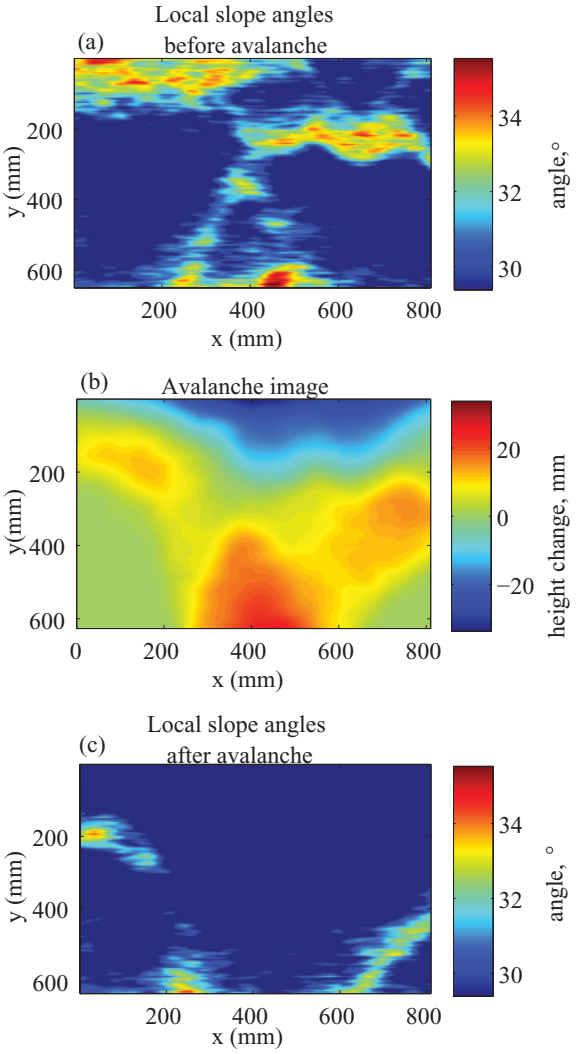

FIG. 17. (Color online) Distribution of the local angles γ on the mung bean pile surface, (a) before a particular avalanche, (c) after this avalanche. Deep blue (dark) indicates relaxed part of the pile, and other colors (bright) indicate part of the pile where $\gamma > \gamma_{\text{pile}}^{\max}$. (b) Change of the pile height by this avalanche is shown. The avalanche moves downward in the figure (from small to large y). Blue (upper dark gray part of the image) indicates regions where particles are removed, and red (lower part of the image) indicates regions where particles are added.

we do observe the start of avalanches in a small range of angles, spanning a few degrees below this value. After the avalanche, the average slope is reduced to a value close to 35°, i.e., below the threshold of 37°, and the instability is relaxed. However, in the area where the avalanche stopped, a new local instability appears due to the accumulation of new grains. In the yellow regions of Fig. 16(c), large values for the local angles have now appeared, with even $\gamma_{\text{local}} > 42°$ (close to the 400 tick mark on the y axis). Thus, even after the avalanche, local critical angles $\gamma_{\text{local}} \simeq \gamma_{\text{local}}^{\max}$ can be found, and the next avalanche is likely to start at or pass through these locally unstable regions. Clearly, even after an avalanche, the pile is still in its critical state. In other words, criticality is preserved by high values of the local angle, while the global angle can be relaxed.

The situation shown in Fig. 16 seems quite general and not limited to the particular type of grain. For all our four grains, we observe similar behavior. Even if the system is not really SOC, like a mung bean pile, the avalanche behavior is quite robust; see, for example, the pile relaxation due to a large avalanche shown in Fig. 17. We thus observe the local structure of criticality. Criticality is always preserved for the pile as a whole, since there are always local regions with $\gamma_{\text{local}} \simeq \gamma_{\text{local}}^{\max}$. Interestingly, in our experiments always $\gamma_{\text{pile}}^{\max} \ll \gamma_{\text{local}}^{\max}$, since usually only a portion of the pile is in a critical state. For example, in Fig. 16(a) less than 15% of the pile has a local angle close to $\gamma_{\text{local}}^{\max}$, but this leads to the avalanche shown in Fig. 16(b) covering 85% of the pile. So even if the system is globally critical it is not necessary for it to be locally critical everywhere. After the avalanche, the percentage of the areas

close to critical state in the relaxed pile [see Fig. 16(c) or Fig. 17(c)] is very small; e.g., in the case of Fig. 16(c) it is less than 2%. Still, due to the presence of even such a small portion of the pile in a nearly critical state, criticality still exists in the pile, and the critical state is globally preserved. This holds true even for non-SOC grains, like the mung beans shown in Fig. 17. Interestingly enough, the only true SOC system, the rice pile, turns out to have the highest angle $\gamma_{\text{pile}}^{\max}$ (and also $\gamma_{\text{local}}^{\max}$) and has also the highest angular fluctuations $\Delta\gamma_{\text{pile}}$. From this one might conjecture that a necessary criterion for the transformation of simple criticality to SOC is a high value of the threshold condition (in this case $\gamma_{\text{local}}^{\max}$), but this is the subject for further investigations.

V. CONCLUSIONS

We have analyzed piles consisting of four different grains of various shapes and aspect ratios. We investigated whether the avalanches on these piles comply to the criteria for self-organized criticality. The criteria for SOC we investigated are a power-law avalanche size distribution, finite size scaling (FSS), and a universal exponent scaling relation (UESR) of exponents of avalanche size, surface roughness, and avalanche fractal dimensions. Although previously systems were sometimes declared to be SOC on the basis of a power-law avalanche size distribution only, we demonstrate here that power-law behavior is possible without FSS and UESR and hence without SOC. In our experiments only one out of three types of grain with power-law distributed avalanches is confirmed to be truly SOC. This is rice, and rice grains have a very high aspect ratio, which enables them to create locally very stable scaffolding structures. It is our conjecture that such local metastability is an important enabling factor for SOC behavior.

From the fluctuation of the angle of the piles, we conclude that larger fluctuations (and thus bigger avalanches) happen in piles consisting of grains with a large aspect ratio. Experimental results also show that only a fraction of the whole pile needs to be near local criticality to cause a system-wide avalanche. Even after a system wide avalanche, the pile locally remains critical, from which a new avalanche may be initiated.

Because of the universality of SOC behavior (see the introduction), we may prudently apply our conclusions to many other systems, natural and manmade. In most cases, SOC behavior is undesirable due to the catastrophic effects of large avalanche-like events, which have a nonvanishing probability to occur due to their power-law distribution. Hence it is important to find out what makes a system SOC and what can be done to get a system out of SOC. Here we presented some findings which may be helpful for this aim, although clearly more work is needed.

ACKNOWLEDGMENTS

This work was supported by the Foundation for Fundamental Research on Matter (FOM), which is subsidized by the Netherlands Organisation for Scientific Research (NWO).

[1] P. Bak, C. Tang, and K. Wiesenfeld, Phys. Rev. Lett. **59**, 381 (1987).
[2] C. H. Scholz, *The Mechanics of Earthquakes and Faulting* (Cambridge University Press, Cambridge, 1991).
[3] S. Hergarten and H. J. Neugebauer, Geophys. Res. Lett. **25**, 801 (1998).
[4] B. Drossel and F. Schwabl, Phys. Rev. Lett. **69**, 1629 (1992).
[5] V. Frette, K. Christensen, A. Malthe-Sørenssen, J. Feder, T. Jøssang, and P. Meakin, Nature (London) **39**, 49 (1996).
[6] C. M. Aegerter, M. S. Welling, and R. J. Wijngaarden, Europhys. Lett. **65**, 753 (2004).
[7] P. Bak and K. Sneppen, Phys. Rev. Lett. **71**, 4083 (1993).
[8] M. Bartolozzi, D. B. Leinweber, and A. W. Thomas, Physica A **370**, 132 (2006).
[9] K. A. Dahmen, Y. Ben-Zion, and J. T. Uhl, Nature Phys. **7**, 554 (2011).
[10] S. Nagel, Rev. Mod. Phys. **64**, 321 (1992).
[11] G. Pruessner and H. J. Jensen, Phys. Rev. Lett. **91**, 244303 (2003).
[12] A. Donev, I. Cisse, D. Sachs, E. A. Variano, F. H. Stillinger, R. Connelly, S. Torquato, and P. M. Chaikin, Science **303**, 990 (2004).
[13] K. Desmond and S. V. Franklin, Phys. Rev. E **73**, 031306 (2006).
[14] G. Lumay and N. Vandewalle, Phys. Rev. E **74**, 021301 (2006).
[15] M. Ramaioli, L. Pournin, and T. M. Liebling, Phys. Rev. E **76**, 021304 (2007).
[16] T. Börzsönyi, T. C. Halsey, and R. E. Ecke, Phys. Rev. E **78**, 011306 (2008).
[17] M. Paczuski, S. Maslov, and P. Bak, Phys. Rev. E **53**, 414 (1996).
[18] C. M. Aegerter, R. Günther, and R. J. Wijngaarden, Phys. Rev. E **67**, 051306 (2003).
[19] A. Corral and M. Paczuski, Phys. Rev. Lett. **83**, 572 (1999).
[20] K. A. Lőrincz, Ph.D. thesis, Vrije Universiteit, 2008, [http://dare.ubvu.vu.nl/bitstream/1871/13052/2/8402.pdf].
[21] K. A. Lőrincz and R. J. Wijngaarden, Phys. Rev. E **76**, 040301(R) (2007).
[22] P. Bak, C. Tang, and K. Wiesenfeld, Phys. Rev. A **38**, 364 (1988).
[23] D. L. Turcotte, Rep. Prog. Phys. **62**, 1377 (1999).
[24] M. Trepanier and S. V. Franklin, Phys. Rev. E **82**, 011308 (2010).
[25] V. Buchholtz and T. Poschel, Physica A **202**, 390 (1994).
[26] S. S. Manna, J. Phys. A: Math. Gen. **24**, 363 (1991).
[27] Yi-Cheng Zhang, Phys. Rev. Lett. **63**, 470 (1989).
[28] K. Christensen, Á. Corral, V. Frette, J. Feder, and T. Jøssang, Phys. Rev. Lett. **77**, 107 (1996).
[29] M. Bengrine, A. Benyoussef, A. El Kenz, M. Loulidi, and F. Mhirech, Eur. Phys. J. B **12**, 129 (1999).
[30] K. Christensen, N. Farid, G. Pruessner, and M. Stapleton, Eur. Phys. J. B **62**, 331 (2008).
[31] J. Feder, Fractals **3**, 431 (1995).

[32] By "small ξ" we mean that a stretched exponent curve constructed with a such value of ξ can be almost perfectly fitted with a power law over the number of orders of magnitude observed in our experiments (roughly four). More precisely, a power-law fit for such curve will yield a $\overline{R}^2$ value larger than 0.99.

[33] A. L. Barabási and H. E. Stanley, *Fractal Concepts in Surface Growth* (Cambridge University Press, Cambridge, 1995).

[34] B. B. Mandelbrot, *The Fractal Geometry of Nature* (W. H. Freeman, San Francisco, 1982).

[35] O. Peters, A. Deluca, A. Corral, J. D. Neelin, and C. E. Holloway, J. Stat. Mech. (2010) P11030.